Investigations of Magnetohydrodynamic Instabilities in the STOR-M Tokamak

C. Xiao, S. Elgriw, M. Dreval, T. Niu[1], A. Pant, D. Rohraff, A. Singh[2], D. Trembach, A. Hirose

Plasma Physics Laboratory, University of Saskatchewan, Saskatoon, Canada

E-mail: chijin.xiao@usask.ca

Abstract. Studies of magnetohydrodynamic (MHD) instabilities in the Saskatchewan Torus-Modified (STOR-M) tokamak have been conducted to examine the mode structures and time evolution during the Ohmic discharges and after compact torus (CT) injection. External discrete Mirnov coils and two pin-hole soft x-ray (SXR) cameras have been used for the studies. The time-resolved frequency component analysis has been performed using wavelets. Fourier-based techniques alongside with singular value decomposition (SVD) algorithm have been employed to analyze the frequency and wavenumber harmonics of the MHD fluctuations. The dominant rotating magnetic structures with poloidal and toroidal modes (4,1) and (2,1) have been identified during typical discharges with an edge safety factor $q \sim 5$. Mirnov and SXR signals were strongly correlated at frequencies in the range of 20-40 kHz. In another experiment, noticeable MHD fluctuation suppression has been observed after the H-mode-like phase transition induced by CT injection. Prior to the L-H back transition, a kink-like instability burst termed gong mode with a poloidal mode number $m = 1$ appears, followed by strong $m = 2$ oscillations.

1. Introduction

MHD instabilities in tokamaks usually grow on resonant magnetic surfaces with rational values of the safety factor q [1], destabilize plasma, and even cause a major disruption of a discharge. It is important to monitor the MHD instabilities and to analyze the features of the fluctuating signals associated with various instabilities in order to identify disruption precursors and to develop remediation strategies. Many diagnostic tools and data processing techniques have been developed to study those fluctuating signals in terms of their temporal evolution and spatial structures expressed by the poloidal and toroidal mode numbers (m, n). Mirnov coils directly measure the magnetic field fluctuations associated with rotating magnetic islands and the soft x-ray (SXR) cameras monitor the variation of the SXR emissivity around the magnetic islands. In the STOR-M tokamak, the MHD activities are monitored by several sets of discrete Mirnov arrays installed at various poloidal and toroidal locations, allowing calculation of the poloidal and toroidal mode numbers (m, n). A new SXR system consisting of two miniature pin-hole cameras has been recently installed in STOR-M [2] to complement Mirnov coil measurements. Morlet wavelet has been adopted to perform time-resolved frequency analysis for transient and non-stationary fluctuating signals [3]. Other tools used include conventional Fourier cross-correlation (FCC) analysis [4], Fourier coefficients decomposition (FCD) in both frequency and wavenumber domains [5], and SVD algorithm [6] for simultaneous decomposition of spatial structures and temporal evolutions of the fluctuation signals.

It has been found in early STOR-M experiments that $m = 2$ Mirnov oscillations were suppressed while $m = 3$ oscillations remained almost unaffected during the H-mode like discharges induced by tangential compact torus (CT) injection [7]. The H-mode-like phase is characterized by a significant increase in the electron density, reduction in H_α radiation intensity, increase in energy confinement time, and reduction in floating potential fluctuations. High SXR emission from the

---

[1] *Department of Modern Physics, University of Science and Technology of China, Hefei, China*

[2] *Department of Physics, Utah State University, Logan, Utah, USA.*

hot plasma core has also been observed after vertical CT injection [8]. However, the magnetic fluctuation signals were measured by pre-connected Mirnov coils measuring either $m = 2$ or $m = 3$ Mirnov oscillations. The 8-bit digitizers did not have a resolution high enough for detailed numerical analysis. In previous CT injection experiments, it has also been noticed that an increase in $m = 2$ Mirnov oscillations occurs before the termination of the transient improved confinement phase, raising a question whether the high amplitude of Mirnov oscillations is a direct or indirect precursor for the H-L back transition in STOR-M [9].

This paper reports the spatial and temporal features of fluctuations observed by Mirnov coil arrays and SXR detector arrays. In particular, detailed analysis of the mode structures of magnetic fluctuations has been performed during the period shortly before the transition from the improved confinement phase triggered by CT injection to the nominal confinement phase.

2. Experimental Setup

The STOR-M tokamak is a small tokamak with a major radius of 46 cm and minor radius of 12.5 cm. STOR-M is equipped with a feedback control system for horizontal position, a 4 mm microwave interferometer for electron density measurements. The plasma parameters during a typical STOR-M discharge are I_p (plasma current) = 20~30 kA, V_l (loop voltage) = 3 V, B_t (toroidal magnetic field) = 0.7 T, n_e (electron density) = $0.5 \sim 2 \times 10^{19}$ m^{-3} and τ_E (global energy confinement time) = 1 ms. The University of Saskatchewan CT injector (USCTI) is used to inject a CT horizontally from the low field side in a direction tangential to the toroidal magnetic field. CTs with a mass of 1 μg, and electron density in the range $1 \sim 4 \times 10^{21}$ m^{-3} are accelerated to velocities up to 150 km/s [10]. The CTs are typically injected into the STOR-M discharge during the plasma current flat-top phase.

MHD oscillations in the STOR-M tokamak have been recorded using two types of Mirnov coils, the pre-connected conventional $m = 2$ and $m = 3$ coils and the discrete coil arrays. Two sets of arrays, each consisting of 12 discrete Mirnov coils with 30° poloidal separation, are mounted at two opposite toroidal locations on thin (0.5 mm) stainless steel bellows sections. The coils are capable of measuring poloidal mode numbers in the range $m \leq 6$. Four sets of toroidal arrays, each consisting of 4 discrete Mirnov coils toroidaly separated by 90° from one another, are used to analyze toroidal modes. The outboard toroidal Mirnov coil array is used to determine the toroidal mode numbers up to $n = 2$.

The SXR system consists of two miniature pin-hole camera arrays [2]. Each SXR camera array consists of 12 photodiodes (IRD AXUV-20EL) collecting SRX emission from 12 fan-like lines of sight. Aluminum foils with a thickness of 1.8 μm (or 7.5 μm Be foils) are used to filter out visible light. The miniature SXR cameras have been installed through two small ports from the top and from outboard at the same toroidal location. Both Mirnov coil and SXR signals are collected by a 14-bit data acquisition system with a sampling rate up to 3 MS/s per channel.

Figure 1 shows the distribution of the Mirnov coil arrays and the vertical and horizontal fan-like lines of sight of two SXR camera arrays.
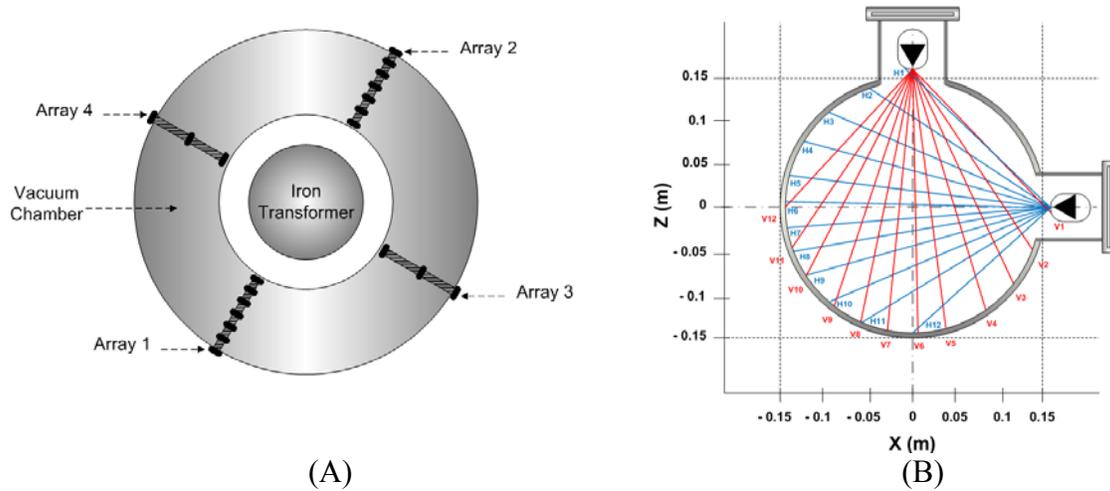
(A)   (B)

Fig. 1. (A) Distribution of Mirnov coil arrays and (B) lines of sight of SXR detector arrays.

3. Experimental results
3.1. Normal ohmic discharge

Figure 2(A) shows the waveforms of the STOR-M discharge #210482. Shown in the diagram are plasma current I_p, loop voltage V_l, electron density n_e, plasma horizontal displacement ΔH, H_α radiation intensity, calculated edge safety factor $q(a)$, magnetic fluctuations dB_ϑ / dt, and SXR radiation intensity from a central chord. The plasma parameters in this discharge are $I_p \sim 20$ kA, $V_l = 3$ V and $B_t = 0.5\text{-}0.7$ T (dropping during the discharge, not included in the diagram). The SXR emission intensity peaks shortly after the discharge current peak and decays as plasma current and density decrease. The edge safety factor value lies between 5 and 6 during the plasma current plateau. Figure 2(B) shows the structures of the dominant $m = 4$ poloidal mode and the associated $n = 1$ toroidal mode as identified by the SVD analysis. The Mirnov oscillation frequency of the (4, 1) mode is about 40 kHz for this discharge.

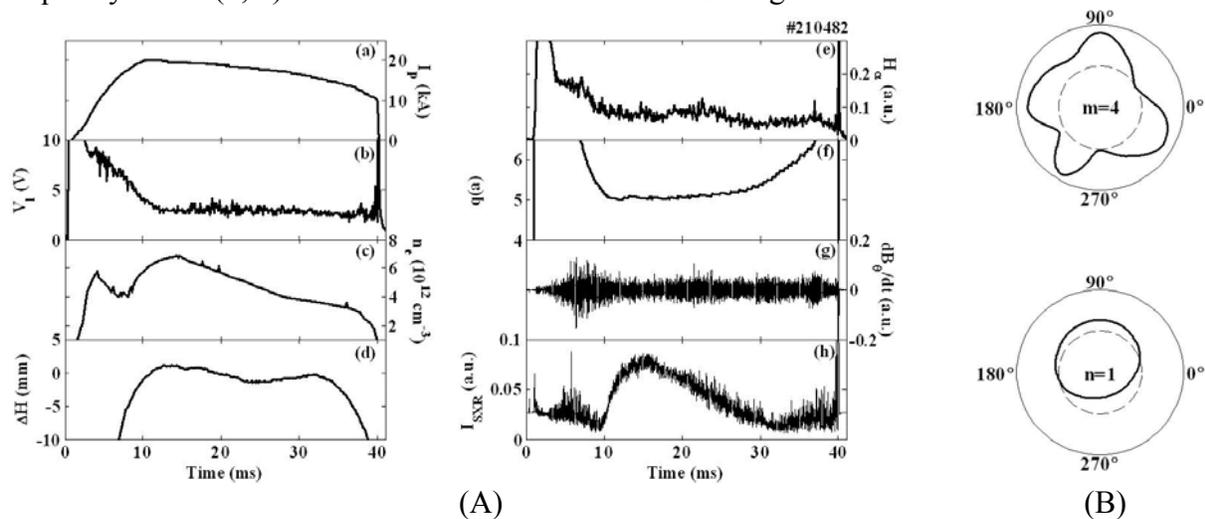(A)   (B)

Fig. 2. (A) Waveforms of (a) plasma current (b) loop voltage (c) average electron density (d) horizontal position (e) H_α emission (f) safety factor (g) Mirnov signal (h) SXR signal. (B) Poloidal m=4 and toroidal n=1 mode structures revealed from the SVD analysis.

Figure 3 shows the expanded traces of the SXR signals from two channels near the plasma center. The V5 shows clear sawtooth oscillations (STOs) associated with the $m = 1$ tearing mode. The V7 channel shows inverted sawtooth oscillations, indicating that the $q = 1$ surface lies between the channels V5 and V7.
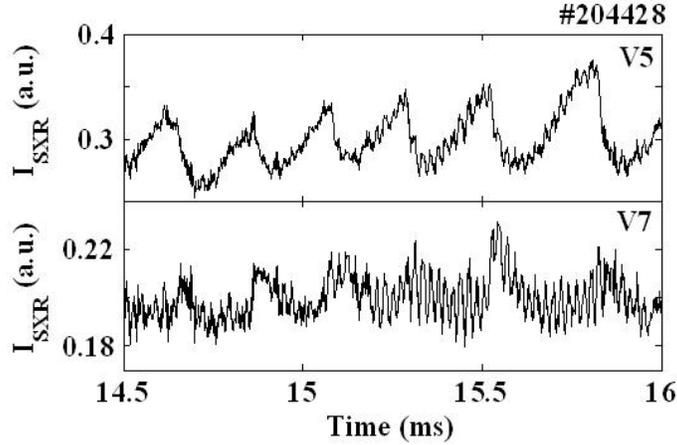

Fig. 3. SXR emission brightnesses measured through two chords near the STOR-M center.

It has also been observed that high frequency oscillations are superimposed on STOs. Those oscillations are highly correlated with the magnetic fluctuations detected by the Mirnov coils. It has also been observed that clear STOs occur only when the magnetic fluctuations are relatively weak. Figure 4 shows the waveform and wavelet power spectra of the magnetic fluctuations and high frequency SXR oscillations during an STO-free phase. Both fluctuations have the same stable frequency about 23 kHz. The relative intensity of the high frequency SXR oscillations decreases as the relative intensity of the magnetic fluctuations increases and vise versa.
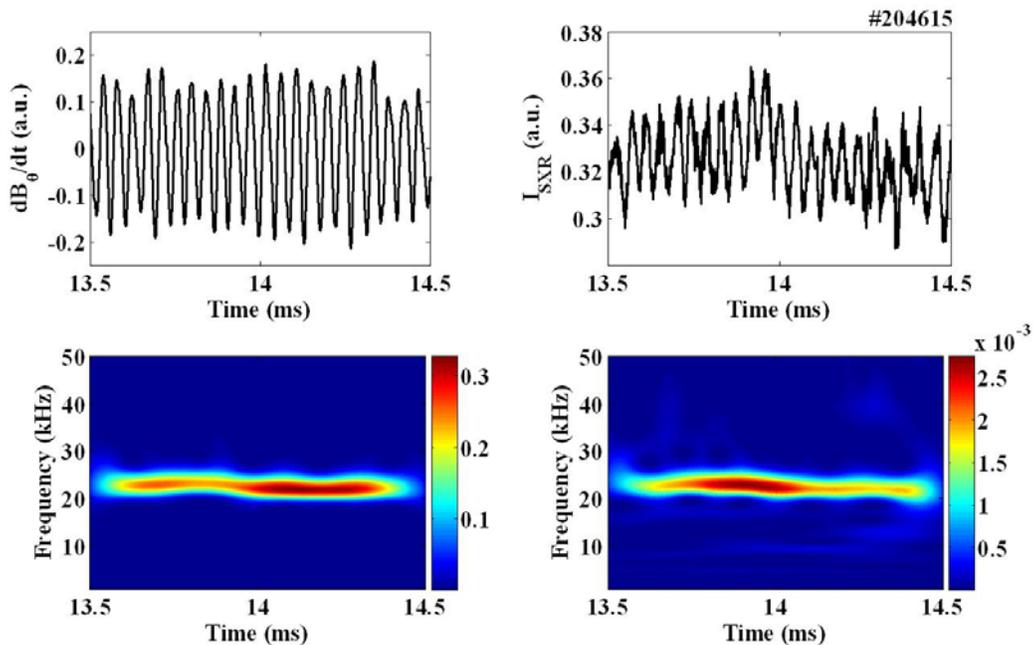

Fig. 4. Top: Mirnov and SXR MHD oscillations. Bottom: Wavelet power spectra.

Figure 5 shows the auto-power spectra of the Mirnov and SXR MHD oscillations. Both spectra peak at the same frequency and the coherence coefficient near that frequency peaks to a value of 0.99. The high coherence of the Mirnov oscillations and SXR emission oscillations suggests that the plasma temperature and/or density within the magnetic islands are quite different from that outside the island.
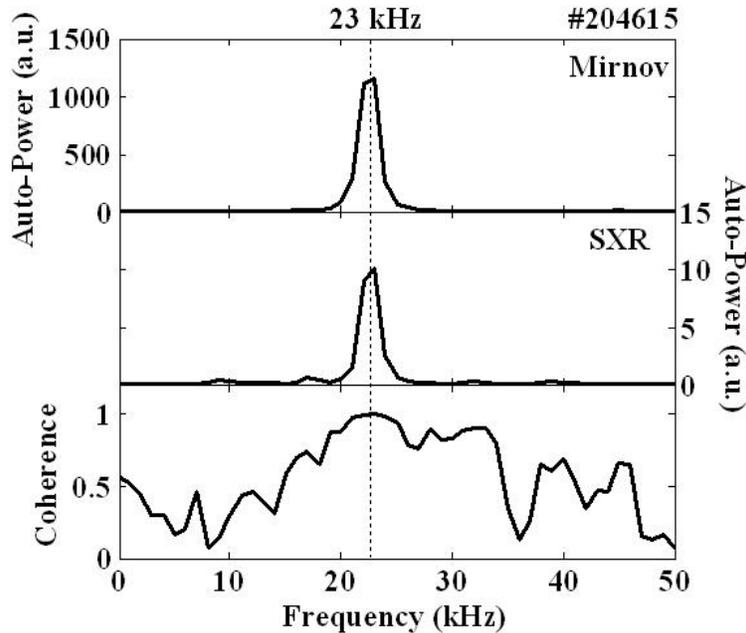

Fig. 5. Auto-power spectra of the Mirnov and SXR MHD oscillations and the coherence spectrum.

3.2. CT injection

Previous CT injection experiments on STOR-M have shown that an improved confinement phase is induced for several milliseconds immediately after CT injection. During this improved confinement phase, the $m = 2$ Mirnov oscillations are significantly suppressed while the $m = 3$ oscillations remain almost unaffected. The $m = 2$ mode reappears before the discharge returns to a low confinement phase [10]. Figure 6 shows the Mirnov oscillations detected by one of the discrete Mirnov coils during a discharge with CT injection (#182960). The noise spike marked on the Mirnov signal at 15.25 ms indicates the instance of compact toroid injection into the tokamak discharge. CT injection caused a phase of suppressed Mirnov oscillations between 15.6 ms and 16.2 ms within the H-mode-like phase. However, the suppression phase was terminated by a spike in the Mirnov signal followed by coherent oscillations which lasted for about 0.4 ms between 16.2 ms and 16.6 ms.

Detailed analyses have been carried out to reveal the features of the increased MHD activities. Figure 7(A) shows the contour plot of the signal amplitudes of a poloidal Mirnov coil array. The regular bright strips indicate a propagating wave along the poloidal direction, corresponding to the rotation of an $m = 2$ magnetic island. The weak $m = 2$ structure can also be seen during the suppressed phase in the diagram before $t = 16.33$ ms. The nature of the propagating $m = 2$ structure along the poloidal direction has also been confirmed by cross-phase analysis of signals

of all Mirnov coil at various locations with respect to a fixed coil. The phase difference increases linearly as the angular angle between the coil and the reference coil increases as shown in Fig. 7(B).
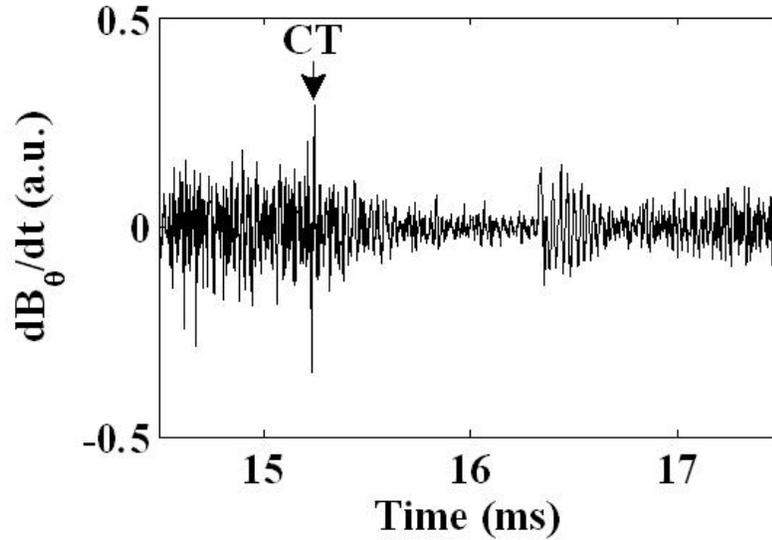

Fig. 6. Mirnov oscillations before and after CT injection.

Figure 7 (A) also shows an $m = 1$ structure around $t = 16.34$ ms for about 0.02 ms. SVD analysis has been applied to the signals of the poloidal Mirnov coil array for the time span from 16.2 to 16.6 ms. The SVD analysis revealed two distinct modes. The first mode has been identified as $m = 1$ mode as it is shown in the top panels of Fig. 8. The temporal evolution shows a short-lived peak. This bursting mode was followed by a magnetic structure $m = 2$ rotating at a frequency of 30 kHz, corresponding to a plasma angular rotation frequency of about 10^4 rad/sec if a rigid body rotation is assumed. The spatial structure and temporal evolution of the $m = 2$ mode are plotted in the lower panel of Fig. 8.
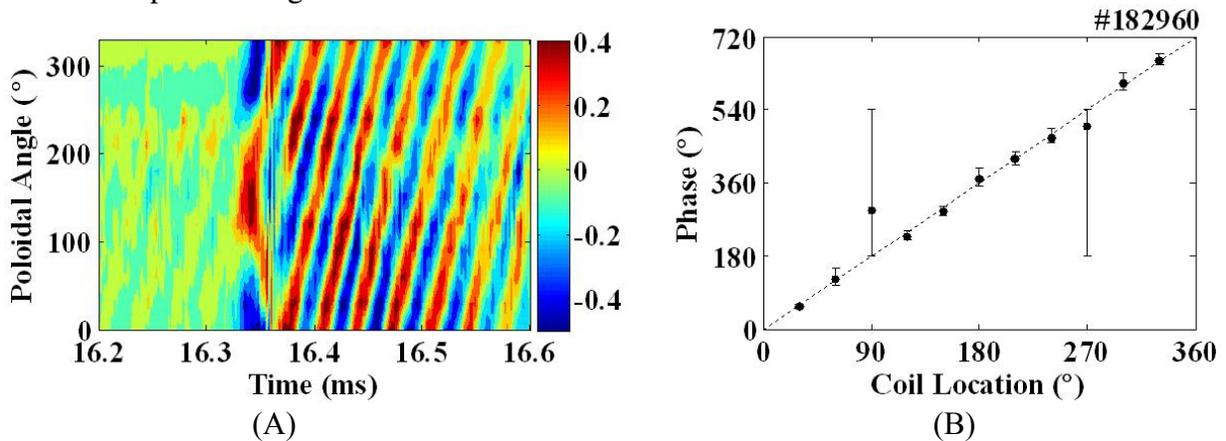

(A)

(B)

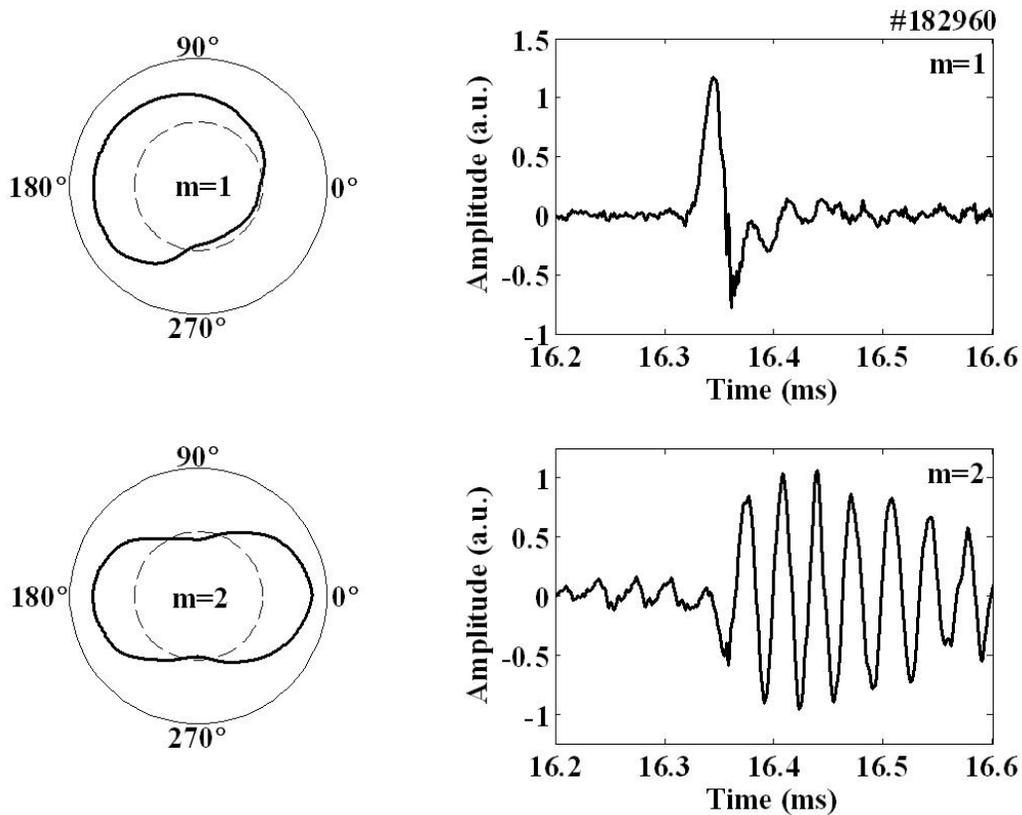*Fig. 7. (A) Contour plot of Mirnov signal amplitudes, and (B) cross-phase of the Mirnov oscillations.*

Fig. 8. The spatial structure and temporal evolution of the bursting m=1 mode (top panels) and the following rotating m=2 mode.

This transient kink-like $m = 1$ instability is termed gong mode [11], by analogy with a gong being hit in its center by a hammer. The gong mode may rotate in poloidal and toroidal directions like any other MHD modes. However, its lifespan (~ 0.02 ms) in STOR-M is shorter than the rotation period which explains its unusual non-propagating behavior. The gong modes have been observed in machines with inverse aspect ratio $\varepsilon = a/R \sim 0.3$ ($\varepsilon = 0.27$ in STOR-M) as the mode coupling in high aspect ratio tokamaks may be responsible for the mode to develop.

Although the toroidal structure of the gong perturbation has been always measured as $n = 1$, its poloidal mode number was usually found to be equal to the integer part of the safety factor at the last closed surface $q(a)$. In the JET tokamak, the m value of gong mode was 4 for $q(a) = 4.2$, though low values of m between 1 and 3 have been transiently observed [5]. The poloidal gong structure was $m = 3$ in the Tore Supra tokamak which agrees with $q(a) = 3.4$ [11]. In STOR-M, the calculated q value at the plasma periphery was $q(a) = 4.9$. However, only a strong $m = 1$ gong mode is identified, indicating that the inner mode may be stronger than the ones at the outer resonant q surfaces with higher mode numbers.

It is not clear at this moment whether the $m = 1$ gong mode is the trigger for the strong $m = 2$ oscillations which may have been the cause for the H-L back transition. When the gong mode was observed there was only one poloidal Mirnov coil array (Array 1 in Fig. 1). An additional poloidal Mirnov coil array (Array 2 in Fig. 1) has been recently installed 180° away from the first

one in the toroidal direction in an attempt to clarify whether the gong mode is localized at a particular toroidal location or appears globally over the entire toroidal column.

4. Conclusions

The MHD oscillations in the STOR-M tokamak have been monitored by discrete poloidal and toroidal Mirnov coil arrays and by two SXR pin-hole cameras. The wavelet, FFT and SVD techniques have been used to perform time-frequency and spatial-wavenumber harmonics analyses on the measured MHD fluctuations. A case study has been considered during the normal ohmic discharge of STOR-M. The (4, 1) mode dominate the discharge with a peak frequency of about 40 kHz. In another discharge, a strong (2, 1) mode at about 23 kHz has also been observed. The Mirnov and SXR fluctuations are highly correlated.

MHD fluctuations have been investigated during an improve confinement phase triggered by tangential CT injection. Significant suppression of MHD fluctuations during the improved confinement phase has been observed. However, MHD activities reappeared prior to the H-L back transition. The reappearance of the MHD activities is led by a kink-like $m = 1$ gong mode burst followed by coherent $m = 2$ oscillations.

Acknowledgement

References:

[1] A. I. Morozov and L. S. Solov'ev, The Structure of Magnetic Fields, In Reviews of Plasma Physics **2**, Consultants Bureau, New York (1966).
[2] C. Xiao, T. Niu, J. E. Morelli, C. Paz-Soldan, M. Dreval, S. Elgriw, A. Pant, D. Rohraff, D. Trembach and A. Hirose, Rev. Sci. Instrum. (in press).
[3] A. Teolis, Computational Signal Processing with Wavelets, Birkhäuser, Boston (1998).
[4] D. E. Smith, E. J. Powers and G. S. Caldwell, IEEE Transactions on Plasma Science **PS-2**, 261 (1974).
[5] P. A. Duperrex, A. Pochelon, A. W. Edwards, J. A. Snipes, Nucl. Fusion **32**, 1161 (1992).
[6] J. S. Kim, D. H. Edgell, J. M. Greene, E. J. Strait and M. S. Chance, Plasma Phys. Control. Fusion **41**, 1399 (1999).
[7] S. Sen, C. Xiao, A. Hirose, and R.A. Cairns, Phys. Rev. Lett. **88**, 185001 (2002).
[8] D. Liu, C. Xiao, A. Singh and A. Hirose, Fusion Energy 2004: Proc. 20th Int. Conf., FT/**P6-38** (2004).
[9] C. Xiao, S. J. Livingstone, A. K. Singh, D. Raju, G. St. Germaine, D. Liu, C. Boucher, A. Hirose, IAEA Fusion Energy, EX/**P4-31** (2006).
[10] C. Xiao, A. Hirose and S. Sen, Phys. Plasmas **11**, 4041 (2004).
[11] T. Dudok de Wit, R. Lima, A.-L. Pecquet, and J.-C. Vallet, Phys. Plasmas **1**, 3288 (1994).